Air Quality, Atmosphere & Health
https://doi.org/10.1007/s11869-021-01119-2

Columnar aerosol types and compositions over peninsular Southeast Asia based on long-term AERONET data

Sheng-Hsiang Wang[1,2] · Hsiang-Yu Huang[1] · Che-Hsuan Lin[1] · Shantanu Kumar Pani[1] · Neng-Huei Lin[1,2] · Chung-Te Lee[2,4] · Serm Janjai[3] · Brent N. Holben[5] · Somporn Chantara[6]

Received: 2 April 2021 / Accepted: 20 October 2021

Abstract

Aerosol chemical components such as black carbon (BC) and brown carbon (BrC) regulate aerosol optical properties, which in turn drive the atmospheric radiative forcing estimations due to aerosols. In this study, we used the long-term measurements from AERONET (Aerosol Robotic Network) to better understand the aerosol types and composition with respect to their seasonal and spatial variabilities in peninsular Southeast Asia (PSEA, here defined as Vietnam, Cambodia, Thailand, Laos, and Myanmar). Two methods (i.e., aerosol type cluster and aerosol component retrieval) were applied to determine the aerosol type and chemical composition during the biomass-burning (BB) season. AERONET sites in northern PSEA showed a higher AOD (aerosol optical depth) compared to that of southern PSEA. Differences in land use pattern, geographic location, and weather regime caused much of the aerosol variability over PSEA. Lower single-scattering albedo (SSA) and higher fine-mode fraction (FMF) values were observed in February and March, suggesting the predominance of BB type aerosols with finer and stronger absorbing particles during the dry season. However, we also found that the peak BB month (i.e., March) in northern PSEA may not coincide with the lowest SSA once dust particles have mixed with the other aerosols. Furthermore, we investigated two severe BB events in March of 2014 and 2015, revealing a significant BrC fraction during BB event days. On high AOD days, although the BC fraction was high, the BrC fraction remained low due to lack of aerosol aging. This study highlights the dominance of carbonaceous aerosols in the PSEA atmosphere during the BB season, while also revealing that transported dust particles and BrC aerosol aging may introduce uncertainties into the aerosol radiative forcing calculation.

Keywords Biomass burning · Aerosol optical properties · Aerosol composition · Black carbon · Brown carbon

Introduction

Atmospheric aerosols, either from natural sources or anthropogenic emissions, perturb Earth's radiation budget directly by scattering and absorbing incoming solar radiation (Charlson et al. 1992; Chylek and Wong 1995; Hassan et al. 2015). Aerosol direct radiative forcing is usually negative at the top of the atmosphere (TOA) under clear sky conditions. However, it can become less negative or even positive with an increase in aerosol absorption, especially over high albedo surfaces (Boucher et al. 2013; Feng et al. 2013; Wang et al. 2007). This aerosol absorption is mainly regulated by the aerosol chemical components and their respective mass fractions. Aerosol chemical components such as sulfate, nitrate, and sea-salt are efficient light scattering components (IPCC 2013), whereas mineral dust (DU), black carbon (BC), and brown carbon (BrC) are principal absorbers of

✉ Sheng-Hsiang Wang
carlo@g.ncu.edu.tw

[1] Department of Atmospheric Sciences, National Central University, Taoyuan 32001, Taiwan

[2] Center for Environmental Monitoring and Technology, National Central University, Taoyuan 32001, Taiwan

[3] Department of Physics, Faculty of Science, Silpakorn University, Nakhon Pathom 73000, Thailand

[4] Graduate Institute of Environmental Engineering, National Central University, Taoyuan 32001, Taiwan

[5] Goddard Space Flight Center, NASA, Greenbelt, MD 20771, USA

[6] Environmental Science Program, Faculty of Science, Chiang Mai University, Chiang Mai 50200, Thailand

Published online: 30 November 2021

solar radiation (Moosmüller et al. 2009). Mixing of aerosols can also change their optical and radiative properties (Forster et al. 2007). Large uncertainties in aerosol radiative forcing estimations still persist on a global as well as regional scale due to knowledge gaps in and the high spatiotemporal variability of aerosol chemical, microphysical, and optical properties (IPCC 2013). Thus, it is essential to gain a better understanding of aerosol chemical composition based on observational studies to reduce these uncertainties (e.g., Van Beelen et al. 2014).

Traditionally, aerosol chemical components can be detected through in situ measurements and offline sampling coupled with laboratory analysis, but these approaches have often focused on surface level sites and are limited in their spatial coverage (Xie et al. 2017), and are not representative of aerosol chemical composition on the global scale (Chen et al. 2019). Field campaigns are typically conducted for weeks to months, thus unable to provide long-term aerosol chemical profile patterns. Moreover, long-term measurement networks are limited to surface measurements. On the other hand, remote sensing techniques have shown enormous potential for characterizing global aerosol absorption using long-term observations of aerosol optical properties (Chen et al. 2019). Providing continuous, long-term, and readily available aerosol optical and microphysical properties, the ground-based worldwide Aerosol Robotic Network (AERONET; Holben et al. 1998, 2001) has been widely used in literature to determine aerosol optical properties over specific source regions (Chu and Ha 2016; Giles et al. 2012; Russell et al. 2010). Furthermore, several studies have also determined columnar aerosol composition based on AERONET observations over different and distinct regions (Bahadur et al. 2012; Chen et al. 2019; Esteve et al. 2012; Schuster et al. 2005; Xie et al. 2014, 2017).

Ever since the Seven South East Asian Studies (7-SEAS)/Dongsha Experiment (Lin et al. 2013) exposed that immense biomass-burning (BB) pollution from peninsular Southeast Asia (PSEA, here defined as Vietnam, Cambodia, Thailand, Laos, and Myanmar) is transported to adjacent oceanic regions and significantly affects the regional climate, there has been intense focus on characterizing the aerosols over northern PSEA. 7-SEAS/BASELInE (Biomass-burning Aerosols & Stratocumulus Environment: Lifecycles & Interactions Experiment) spring campaigns during 2013–2015 were conducted to primarily understand the impacts of BB emissions on surface-atmosphere energy budgets (Lin et al. 2014; Pani et al. 2016, 2018; Wang et al. 2015) over the northern PSEA region. Although the complex aerosol environment of northern PSEA, particularly during the BB season, has been extensively investigated within the 7-SEAS framework, the role of absorbing aerosols on the environment is still unclear. Therefore, the primary objective of this study is to understand the seasonal and spatial differences of aerosol optical properties in PSEA, including absorption and aerosol chemical components in BB-influenced smoke haze, by using long-term AERONET direct sun measurements and inversion products. The role of BB-derived absorbing aerosols is thoroughly investigated in this study.

Methodology

Site description

Figure 1 shows the AERONET sites used in this study. In addition to 5 permanent AERONET sites, namely Son La (SL), Chiang Mai (CM), Ubon Ratchathani (UR), Silpakorn Univ (SU), and Bac Lieu (BL), we deployed one temporary site at Doi Ang Khang (DAK), during the 7-SEAS/BASELInE spring campaigns (Tsay et al. 2016). The DAK site (in northern Thailand) is a meteorological station located in the Fang District of Chiang Mai Province, and on a mountain range along the Thai-Myanmar border at an elevation of 1536 m above sea level (a.s.l.) (Wang et al. 2015). Because this site is surrounded by forest and farmland, smoke emitted from agricultural burning and forest fires have occasionally been observed near the site. Next to DAK, the CM site (in northern Thailand) is located at the meteorological station near Chiang Mai airport. The air quality of this site is mainly affected by urban emission and agricultural burning transported from the surrounding areas. The SL site (in northern Vietnam) is situated in a valley surrounded by mountains. The population of Son La is approximately 200,000 people, suggesting the SL site may receive considerable local pollutants. The UR site (in north-eastern Thailand) is located at the meteorological station near Ubon Ratchathani airport.

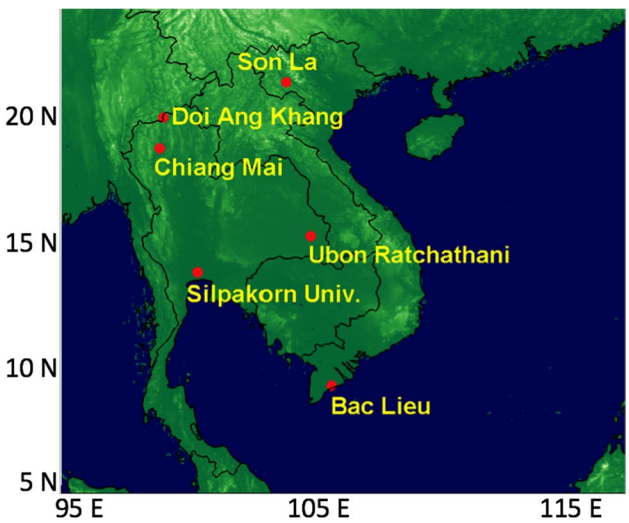

Fig. 1 A topographic map with the location of AERONET stations in the study domain

Agricultural burning and urban emission are the main sources of air pollution in this area. The SU site (in southern Thailand) is located at Silpakorn University in Nakhon Pathom Province, which has a population of ~ 920,000 people; thus, the SU site is heavily impacted by urban emissions. The BL site (in southern Vietnam) is located at Bac Lieu Province. Because the site is close to the South China Sea, the air quality is affected by oceanic particles. Here we separated the six sites into two categories: DAK, CM, and SL sites in northern PSEA, and UR, SU, BL sites in southern PSEA.

The DAK dataset spanned from January to April during 2013–2015. The datasets for the other five sites were of different lengths, but all ended on December 31, 2017. The starting date for CM, SL, UR, SU, and BL sites were January 1 in 2008, 2012, 2007, 2010, and 2006, respectively.

AERONET measurements

AERONET deploys CIMEL Electronique CE-318 Sun-sky radiometers to measure the spectral direct-beam solar radiation as well as directional diffuse radiation along the solar almucantar (Holben et al. 1998, 2001). The direct-beam solar radiation measurements (i.e., direct sun measurement) were used to determine the columnar aerosol optical depth (AOD or τ) in eight spectral channels (340–1020 nm) with a temporal resolution of approximately 15 min. The extinction Ångström exponent (EAE or α) is another derived quantity and is typically used to describe the spectral dependence of AOD. In addition to measuring direct solar irradiance, the sun-sky radiometer measures the sky radiance at four wavelengths (440, 675, 870, and 1020 nm) along the solar almucantar (i.e., at a constant solar zenith angle, with varied azimuth angles). For quality control, the solar zenith angles were restricted to > 50° (i.e., in early morning and late afternoon) and a minimum AOD (440 nm) of 0.02 (Sinyuk et al. 2020). Sky radiance measurements were used to retrieve additional columnar aerosol properties including the volume size distribution, phase function, real and imaginary components of the refractive index (RI), particle effective radius (r_{eff}), single-scattering albedo (SSA), and the asymmetry factor (g), which are typically computed using AERONET inversion algorithms (Dubovik et al. 2000).

Aerosol type classifications

Two methods (i.e., aerosol type cluster and aerosol component retrieval) have been applied to determine the aerosol type and chemical composition during the BB season. We adopted the aerosol type cluster method from Giles et al. (2012), which used average values of the aerosol optical properties across 19 source-specific areas and delineated four aerosol types (i.e., dust, urban/industrial, biomass burning, and mixed) based on a cluster analysis. In our study, the cluster analysis was mainly based on extinction AE and SSA, as shown in cf. Figure 11(c) of Giles et al. (2012).

For the aerosol component retrieval, we used the aerosol composition model described in Li et al. (2013) and Xie et al. (2017). Xie et al. (2014) tested three different internal mixing models (Maxwell–Garnett, Bruggeman, and volume average mixing), and determined that Bruggeman was more suitable for dust events, Maxwell–Garnett was better for haze events, and volume average mixing was the best choice for clean air situations (low aerosol loading). Then, Xie et al. (2017) pointed out that, due to the aerosol hygroscopic growth process, the relation between water and other components must be considered, which was most similar to the assumptions in the Maxwell–Garnett model. Considering the biomass-burning aerosol components and the weather condition in PSEA, we selected the Maxwell–Garnett mixing assumption for our study. The aerosol composition model established in this study includes BC, BrC, DU, ammonium sulfate-like (AS), and aerosol water content (WA). We constrained the Maxwell–Garnett (MG) model with aerosol optical property data from AERONET and solved it as a cost function (Fig. 2). The forward model describes the simulation of refractive indices from aerosol composition and mixing states. The dielectric functions are calculated using the following relations (Bohren and Huffman 1998), and a look-up table of refractive indices of typical aerosol components is provided in Table 1.

$$\varepsilon_j = \left(n_j + k_j i\right)^2 \tag{1}$$

$$\varepsilon_m = \left(n_m + k_m i\right)^2 \tag{2}$$

We calculated the MG dielectric function $\varepsilon_{\mathrm{MG}}$ by using the dielectric functions of components and derived the real refractive index ($n_{\mathrm{MG}}^{\mathrm{cal}}$) and imaginary refractive index ($k_{\mathrm{MG}}^{\mathrm{cal}}$) of the mixture from the MG dielectric function (Bohren and Huffman 1998; Xie et al. 2017):

$$\varepsilon_{\mathrm{MG}} = \varepsilon_m \left[1 + \frac{3\sum f_j \left(\frac{\varepsilon_j - \varepsilon_m}{\varepsilon_j + 2\varepsilon_m} \right)}{1 - \sum f_j \left(\frac{\varepsilon_j - \varepsilon_m}{\varepsilon_j + 2\varepsilon_m} \right)} \right] \tag{3}$$

$$n_{\mathrm{MG}}^{\mathrm{cal}} = \sqrt{\left|\varepsilon_{\mathrm{MG}}\right| + \mathrm{real}(\varepsilon_{\mathrm{MG}}))/2} \tag{4}$$

$$k_{\mathrm{MG}}^{\mathrm{cal}} = \sqrt{(\left|\varepsilon_{\mathrm{MG}}\right| - \mathrm{real}(\varepsilon_{\mathrm{MG}}))/2} \tag{5}$$

where f_j indicates the volume fraction of the jth component in the mixture; ε_j and ε_m are the dielectric functions of the jth component (BC, BrC, DU, AS) and the aerosol water

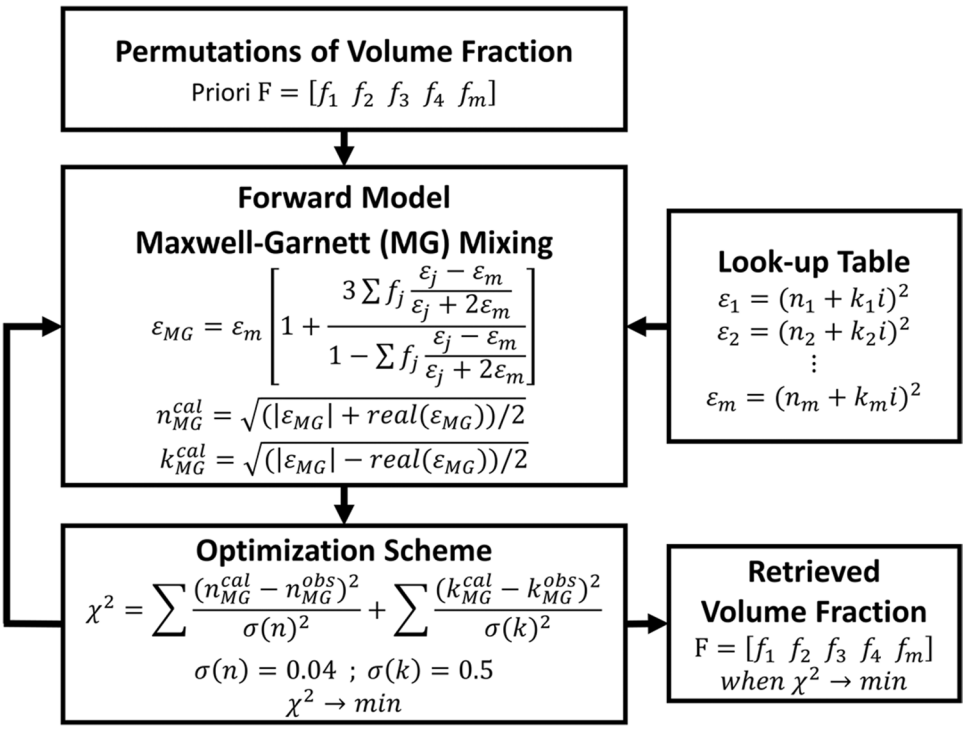

Fig. 2 Schematic diagram of the approach used in this study to calculate the volume fractions of aerosol compositions

content (AW), respectively. Note that the complex refractive index spectra, especially for BC and BrC, are still quite uncertain in the current aerosol optics research, and vary widely across studies (shown in Table S1). The total modeling residual between model ($n_{\mathrm{MG}}^{\mathrm{cal}}$, $k_{\mathrm{MG}}^{\mathrm{cal}}$) and observation ($n_{\mathrm{MG}}^{\mathrm{obs}}$, $k_{\mathrm{MG}}^{\mathrm{obs}}$) was quantified by a cost function (χ^2) based on the least-squares principle:

$$\chi^2 = \sum \frac{\left(n_{\mathrm{MG}}^{\mathrm{cal}} - n_{\mathrm{MG}}^{\mathrm{obs}}\right)^2}{\sigma(n)^2} + \sum \frac{\left(k_{\mathrm{MG}}^{\mathrm{cal}} - k_{\mathrm{MG}}^{\mathrm{obs}}\right)^2}{\sigma(k)^2} \quad (6)$$

where the superscript cal and obs denote modeled (calculated from the forward model) and observed (derived from AERONET measurements) parameters, respectively. The real and imaginary parts of the refractive index are weighted by a factor ($\sigma(n), \sigma(k)$) in the cost function equation to give parameters with higher accuracies and greater contributions. The standard deviations of refractive indices used in this study are 0.04 ($\sigma(n)$) and 0.5 ($\sigma(k)$) (Xie et al. 2017).

Xie et al. (2017) show generally good consistency between remotely estimated and measured components (e.g., correlation coefficients for BC, BrC, AS, and $PM_{2.5}$ were 0.78, 0.8, 0.82, and 0.88, respectively). Finally, we obtained the fraction of aerosol components by minimizing the cost function (χ^2). In Fig. 3, we show the comparison results between the retrievals and aerosol chemistry measurements from February 22 to April 8, 2013. The aerosol chemistry data was adopted from a previous study (Lee et al. 2016). According to aerosol chemistry observation, the retrieval aerosol types underestimated BrC and overestimated DU. Overall, the correlation coefficient between component retrieval and chemical sampling was 0.6 at DAK.

Table 1 Microphysical parameters of aerosol components used in this study, including refractive index (RI) at each wavelength, and density. RI values for different aerosol components at various wavelengths are from Xie et al. (2017)

Aerosol component	RI (440 nm)	RI (670 nm)	RI (870 nm)	RI (1020 nm)	ρ(g cm^{-3})
BC	1.85–0.71i	1.85–0.71i	1.85–0.71i	1.85–0.71i	2.0
BrC	1.57–0.063i	1.55–0.003i	1.54–0.001i	1.54–0.001i	1.8
DU	1.54–0.008i	1.52–0.005i	1.51–0.003i	1.51–0.003i	2.6
AS	1.535–10^{-7}i	1.525–10^{-7}i	1.52–10^{-7}i	1.53–10^{-7}i	1.76
WA	1.33–0i	1.33–0i	1.33–0i	1.33–0i	1.0

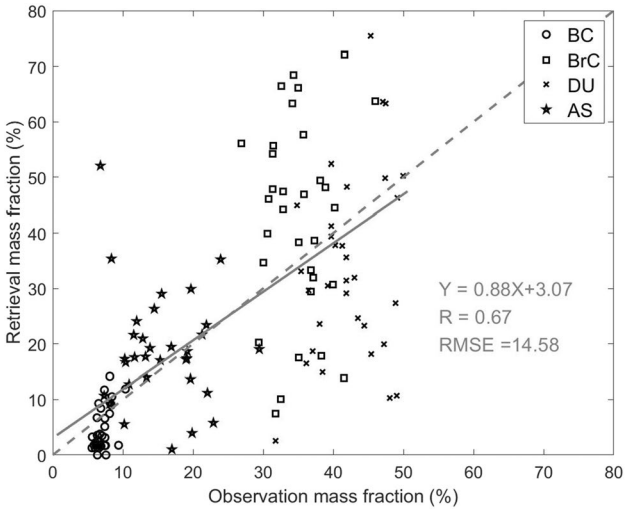

Fig. 3 The comparison between retrievals and observed mass fractions. The observation mass fraction was estimated from daily particulate matter samplers from February 22 to April 8, 2013 (Lee et al. 2016)

Results and discussion

Long-term variability at 6 AERONET sites

BB aerosols are the predominant type of aerosol over PSEA during spring months (Wang et al. 2007; Punsompong et al. 2021). As shown in Fig. 4, the long-term data analysis revealed that the monthly mean aerosol optical depth (AOD) was higher in the months of March and April than in the rest of the months, as observed by all AERONET sites in the region. This finding indicates the influence of regional BB activities, as is also shown by the FMF trends. Fine-mode particles (particle size approximately < 1 μm) are mainly caused by the increase of aerosol loading over PSEA. Due to the spatial differences of geography, land use patterns, and weather regimes, the AERONET sites in northern PSEA show a higher AOD compared to that of southern PSEA. In comparison to the yearly-mean aerosol optical properties, lower single-scattering albedo (SSA) and higher fine-mode fraction (FMF) values in February and March suggested the domination of smaller and stronger absorbing particles during this period. This result is consistent with in situ and satellite measurements described by 7-SEAS field deployments (Lin et al. 2014; Wang et al. 2015). Interestingly, we found that the peak BB month (i.e., March) in northern PSEA may not coincide with the lowest SSA. The possible reasons for the cause are discussed in the following sections.

According to the climate classification by Yen et al. (2013), the PSEA climate could be identified as three seasons: wet season (May to October), dry and cold season (November to January), and dry season (February to April). Figure 5 shows an M-shaped (i.e., fine and coarse modes) particle size distribution for three seasons derived from AERONET observation at the 6 sites during the

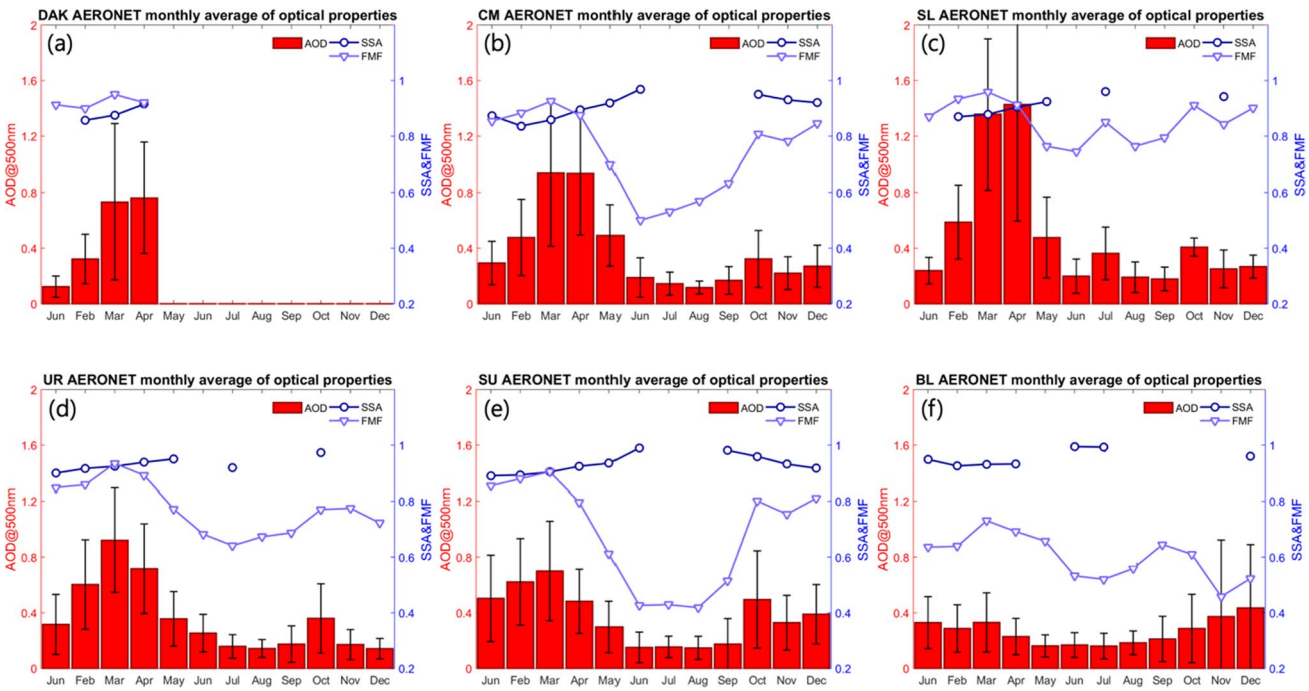

Fig. 4 Monthly variation of aerosol optical properties in PSEA

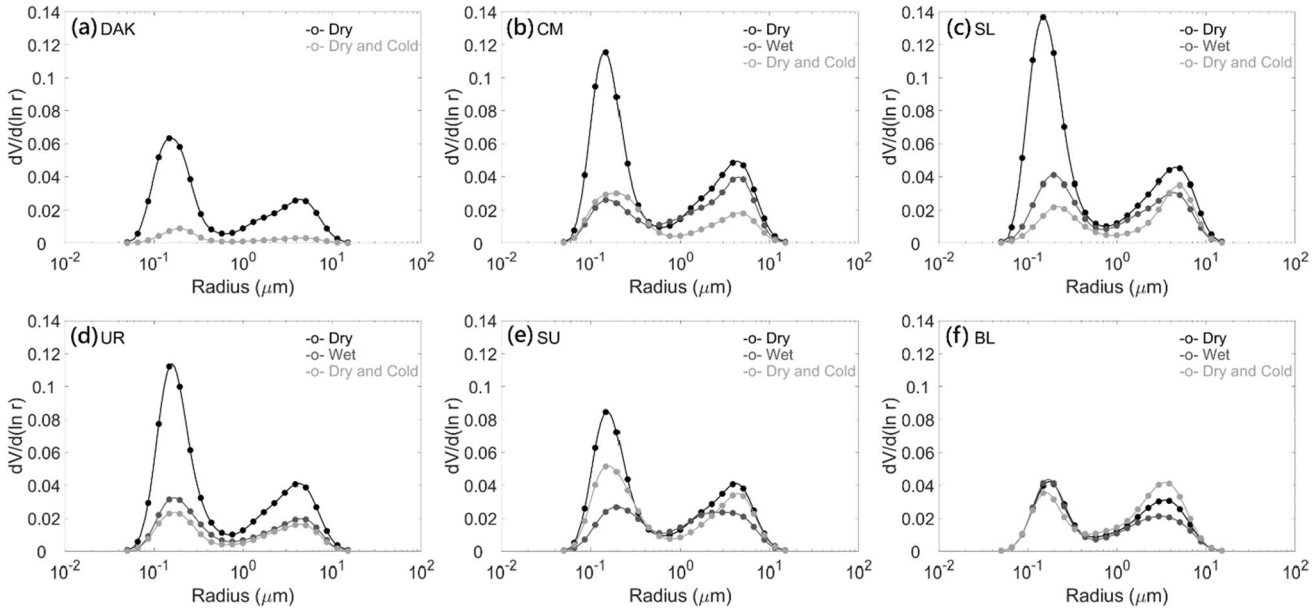

Fig. 5 Particle size distributions over PSEA during three different seasons

study period. Fine-mode particles are generally produced from anthropogenic activity, while coarse mode particles are mainly derived from natural sources. The BL site exhibited less seasonal variation. Except for BL, the rest of the sites showed a pronounced quantity of particle number, especially for fine-mode particles, during the dry season when large amounts of fine BB particles are released into the atmosphere. The weather regimes coupled with land use activities predominate drive the regional variability of aerosols in the dry season. Particle size distributions in wet and dry-and-cold seasons showed a similar pattern at the three eastern sites (i.e., SL, UR, and BL), where coarse mode and fine particles were similar, which was also supported by the FMF values shown in Fig. 4. On the other hand, CM and SU revealed a higher fraction of coarse mode particles in the wet season. The long-range transport of dust particles from the semi-arid regions over northwest India (e.g., Pani et al. 2016) may have influenced the columnar aerosol loading at CM and SU. Overall, the difference in land use patterns, geographic location, and weather regimes may have caused the aerosol variability over PSEA.

Dominant aerosol type in dry season

Aerosol types for each AERONET site in dry season were further discussed using the aforementioned cluster analysis method (Giles et al. 2012). Based on current research results (Lin et al. 2014; Wang et al. 2015), the predominant aerosol type in the dry season is BB; however, site-to-site variation occurs due to the mixing with local pollutants. Figure 6 shows the scatterplot of SSA and EAE. We used 0.1 as the resolution of EAE and 0.01 as the resolution of SSA, and each contour represented the number density of data points. According to Giles et al. (2012), the cluster analysis can be applied to categorize aerosols into four types: dust, urban/industrial, biomass burning, and mixed. The ideal range to represent each aerosol type is marked with an oval and dust type was ignored in Fig. 6 due to its EAE value being low than 0.5 and out of figure range.

As shown in Fig. 6, the CM and SU sites have a higher number of data points. The scatter distribution of CM and SU appeared to be similar, but CM showed more data distributed at lower SSA value. The cluster group with lower SSA might suggest the influence of local anthropogenic pollution. Among the 6 AERONET sites, DAK was selected as representative of a BB near-source region. The cluster analysis results for DAK showed a large area with a number density up to 3.5%, suggesting this was a common optical property of BB aerosols in the dry season. However, this aerosol characteristic was different than the typical aerosol type values suggested by Giles et al. (2012), which defined a representative range based on worldwide selected AERONET sites. Regarding BB, they applied data from Africa savanna or grassland areas, which might have inherently different characteristics from the BB in PSEA. BB aerosols observed at DAK showed generally lower EAE, and much lower EAE for a higher SSA range, as compared to Giles et al. (2012). We suspect

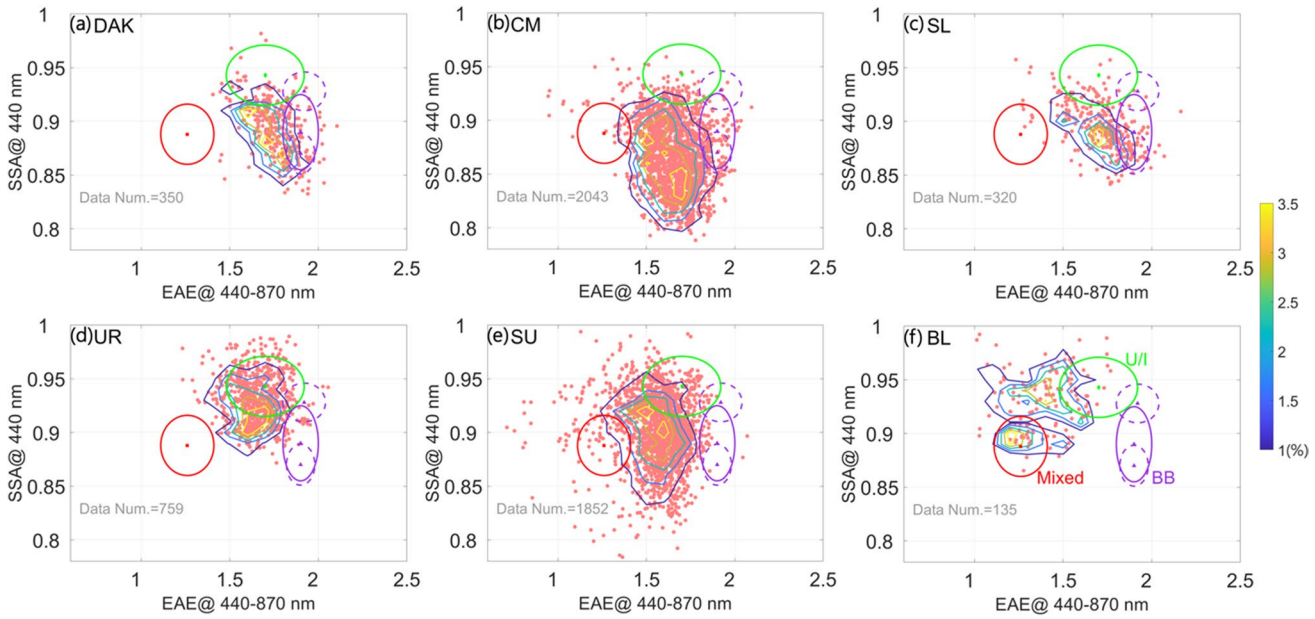

Fig. 6 Cluster analysis of aerosol type over PSEA during January–April (dry season). The oval mark represents the ideal range for three kinds of aerosol types as suggested by Giles et al. (2012). The contour line denotes data density

that dust particles transported at higher levels might have contributed to the columnar aerosol loading and caused the difference. A similar distribution pattern to DAK was also found for SL and UR. According to BL site cluster analysis, a mixed aerosol type with low absorbance was determined during the dry season in southern PSEA.

Aerosol chemical components over northern Thailand in dry season

To gain a better understanding of a mixture of BB aerosols over northern Thailand, we further applied the aerosol refractive index to retrieve various aerosol components. Table 2 shows the fraction of aerosol components in each month at CM. The AERONET level 2.0 data was used for the aerosol component determination (Table 2), but the level 1.5 data was used during July to September, due to lack of the data points. A large fraction of absorbing aerosols was observed in February (BC ≈ 7% and BrC ≈ 43%) and March (BC ≈ 5% and BrC ≈ 38%), reflecting the signature of BB aerosols. DU contributed a major fraction in aerosol components throughout the year, especially from May to December, which includes the wet season and a low aerosol loading period. The dust particles may have been transported from Thar Desert or even Middle Eastern deserts via westerlies within the free troposphere to PSEA. Road dust and farming dust from local emissions could also have caused a high DU fraction. More detailed studies should be performed to clarify the sources of dust in the future. AS usually indicates local industrial or city emissions. The fraction of AS was low in each month, except for July and August, when the lowest AOD was observed (Fig. 4b). We suggest that a high AS fraction in July and August was due to steeply lower contributions from BB and DU.

The variation of aerosol chemical components in the dry season is further discussed. The highest BC and BrC fractions were observed in February when the dry season started. The pronounced increase of BC and BrC reasonably reflected the lowest DU, AS, and WA fractions in February as compared to other months. In March, although the AOD was higher (Fig. 4b) the sum of BC and BrC fractions was lower compared to February. We

Table 2 Fraction (%) of the aerosol component in each month at Chiang Mai (CM)

	Jan	Feb	Mar	Apr	May	Jun	Jul	Aug	Sep	Oct	Nov	Dec
BC	3.1	6.6	5.4	1.2	0.4	0	0.8	2.1	1.7	0.2	0.4	0.8
BrC	41.3	42.8	37.8	40.1	27.2	1.6	14.1	21.8	21.6	25.1	27.7	35.4
DU	26.5	24.3	28.5	30.6	40.3	56.4	37.8	35.6	37.3	41.3	42.0	33.8
AS	17.8	16.3	17.6	16.7	19.6	24.2	30.8	28.9	23.5	18.1	18.2	17.6
WA	11.1	9.7	10.4	11.1	12.2	17.5	16.2	11.3	15.7	15.0	11.5	12.1

further calculated the ratio of BC fraction to (BC + BrC) fraction and found that values (~ 0.13) are close in both months, suggesting the BB characteristics are similar. A higher DU fraction was determined in March. The contribution of dust particles may have modulated the aerosol composition, as well as aerosol optical properties in the peak BB month of March.

Aerosol optical properties and chemical components during BB events

In this section, we further investigated the detailed spatiotemporal variation of aerosol optical properties and chemical components during two severe BB events (i.e., March 19–23, 2014, and March 8–12, 2015) observed at CM and DAK sites. AOD values reached 3 and 2.5, respectively, in these two events (Fig. 7). We identified several common characteristics of event development. Regarding daily variation, the AOD increased steadily with decreasing EAE before reaching event peak days (i.e., March 21, 2014, and March 10, 2015); after the event peak day, AOD decreased but EAE stayed in the low-value range (1.4–1.6). A lower EAE value indicated relatively large particles, which might be due to particle aging, mixture, and growth during a long-lasting event. Both sites illustrated strong diurnal patterns but with time shifts due to station elevation and geographic location differences. CM showed a higher AOD value than DAK in the early morning, but then shifted in the afternoon as the AOD value became higher at DAK than at CM. According to the mountain and valley breeze effect, the BB aerosols which were produced during the previous day would have been trapped in the Chiang Mai valleys by the nocturnal stable boundary layer until early morning. Higher AOD at DAK in the afternoon was due to fresh BB plumes from nearby sources and pre-existing BB aerosols lifted from the valley to the mountain site via planetary boundary layer development. A relevant discussion about the diurnal patterns also can be found in our previous publication (Wang et al. 2015).

Figure 8 shows the MODIS fire counts during the BB event days. The total numbers of daily fire count were calculated within the 2° × 2° domain around DAK and CM. As a result, the daily fire counts were significantly higher in the event peak days (i.e., March 21, 2014, and March 10, 2015) or in the afternoon the day before. More fresh BB aerosols were expected to be observed on the event peak days. Furthermore, the daily variation of retrieval aerosol components is shown in Fig. 9. At DAK, results show a higher BC fraction on the event peak days, implying abundant fresh aerosols emitted from nearby sources. Interestingly, the BrC fraction tended to be lowest on the event peak days, although the BrC fraction significantly increased the next day. This variation of BC/BrC ratios was due to the emission phase. The initial flaming burning phase (i.e., on event peak days) emits mostly BC, while the smoldering phase on the ensuing days emits mostly BrC (e.g., Chen et al. 2006, 2007). A similar feature had also been observed for levoglucosan (a well-known chemical tracer for BB) surface concentrations

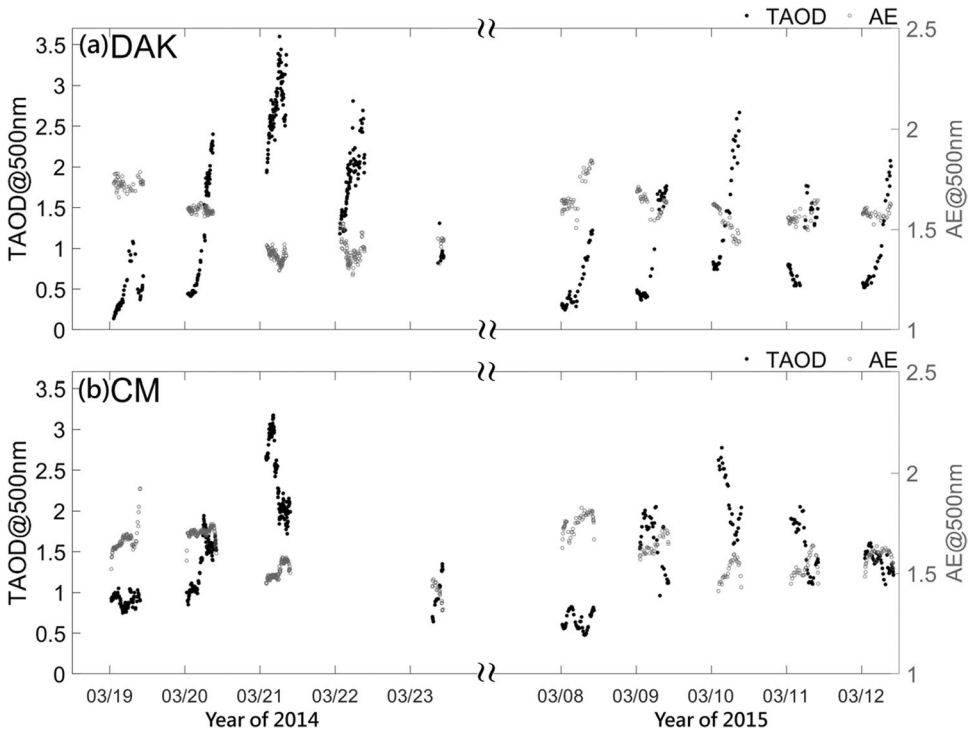

Fig. 7 The AOD and AE variations during the two selected events at **a** DAK and **b** CM stations

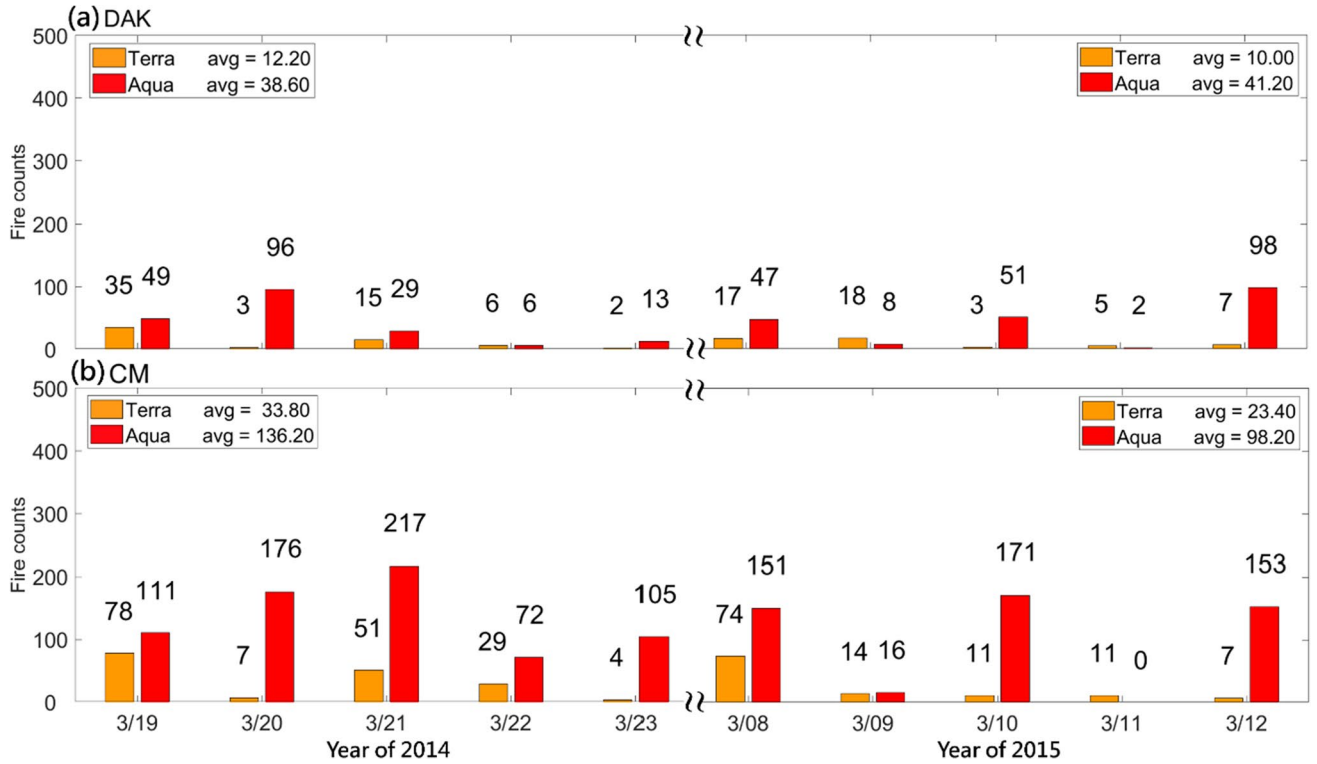

Fig. 8 Fire counts obtained from MODIS instrument onboard Terra and Aqua satellites during the two selected BB events. The daily fire count was calculated within the 2°×2° domain around **a** DAK and **b** CM

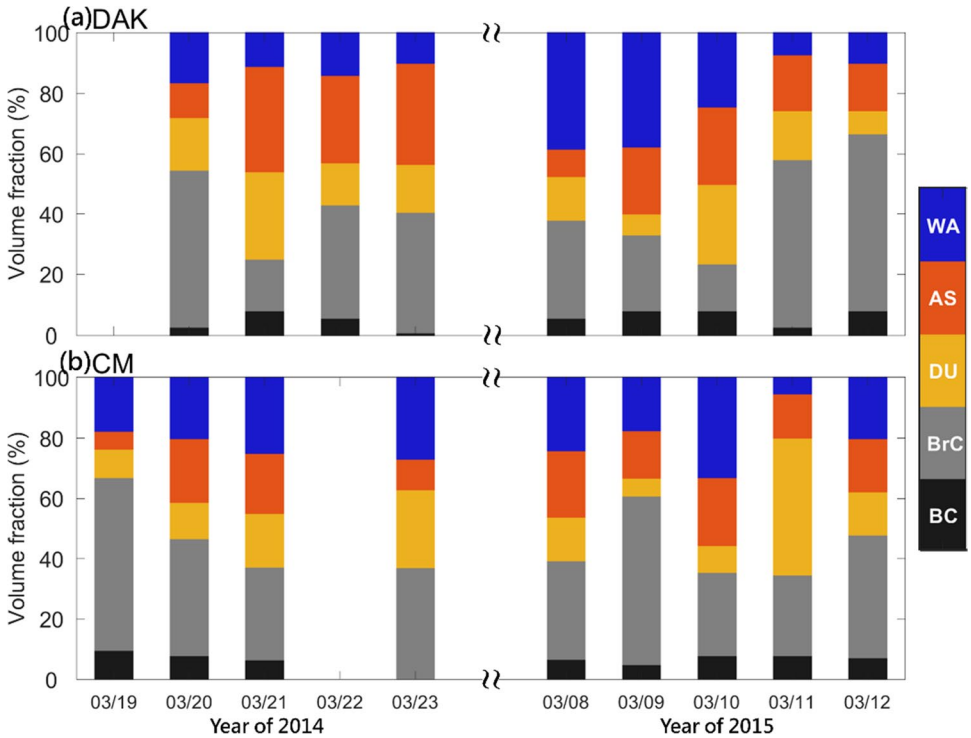

Fig. 9 Aerosol components retrieved from AERONET data during the two selected BB events at **a** DAK and **b** CM stations

over the CM site (e.g., Pani et al. 2018), where decreased BrC fractions were accompanied by an increase of AS and DU fractions. There was no specific tendency of DU fraction during event days, suggesting the input of dust particles in the atmospheric column was variable. Therefore, the transformation and mixing between BrC and AS are further discussed. Before reaching the BB event peak day, aerosol aging and mixing processes occurred under stable weather conditions and adequate solar radiation. We think most BrC particles might be aggregated and externally mixed with AS particles (a.k.a., aerosol aging). Our retrieval method does not consider the complicated mixing state and growth of aerosols; therefore, interpretation of the computational results should be done with caution.

Based on our assessment, we found that the presence of carbonaceous aerosols varied with event evolution. In the early stage of the BB event, sparse fires emitted fresh BC and BrC aerosols with smaller particle sizes (i.e., higher EAE and higher FMF). Those aerosols were suspended in the air and underwent aging, which caused a larger particle size and decreased BrC concentration. Note that, for the absorbing particles (high fraction of BC and BrC), the EAE included a significant absorption component, which for BrC is highly wavelength dependent (Moosmüller and Chakrabarty 2011). Aged BB aerosols existed in the region for 2–3 days, which was proven by a gradual increase of AOD and a decrease of EAE. On the event peak day, the BrC fraction reached its lowest value whereas AS had increased. Significant amounts of fresh BC and BrC aerosols were emitted on the event peak day; however, only BC particles immediately reflected a high fraction on that day. BrC aerosols displayed a large fraction on the next day.

Concluding remarks

In this study, we investigated the aerosol type and optical properties in terms of seasonal to spatial variabilities over peninsular Southeast Asia (PSEA) based on the long-term measurements from 6 sun photometer AERONET (Aerosol Robotic Network) sites. The role of absorbing aerosols (BC and BrC) related to biomass-burning (BB) activities in northern Thailand was studied. To quantify aerosol characteristics, an aerosol type classification method and an aerosol chemical component retrieval method were applied. Furthermore, applying a case analysis (March 19–23, 2014, and March 8–12, 2015), the characteristic aerosol types and chemical components during BB events were also depicted in this study. Those results are summarized as follows:

- AERONET sites in northern PSEA show a higher AOD compared to southern PSEA, where the different weather regimes and land use activities drive the regional variability of aerosol in the dry season (February to April).
- BB aerosols are the predominant type of aerosol over PSEA in February to March. Lower single-scattering albedo (SSA $\approx$ 0.82) and higher fine-mode fraction (FMF $\approx$ 0.95) values imply particles are finer and stronger absorbing during this period. The retrieved aerosol mass indicated high fractions of absorbing aerosols (BC $\approx$ 5% and BrC $\approx$ 40%). However, we also found that the high AOD month (i.e., March) in northern PSEA may not coincide with the lowest SSA once dust particles have mixed with the other aerosols. The contribution of dust particles can modulate aerosol compositions, as well as aerosol optical properties in the peak BB month of March.
- The long-range transport of dust particles from the Thar Desert could have an influence on columnar aerosol loading over PSEA. The dust particles may transport from upwind deserts via westerlies through the free troposphere to PSEA.
- According to the BB event analysis, on the high AOD day, the BC fraction was higher due to fresh emissions from flaming burning, whereas the BrC concentration showed a lower value and then increased in the ensuing days due to smoldering, burning, and photochemical aging. Therefore, a lowest SSA value might not occur at event peak day.
- This study provides a new insight on how transported dust particles and BrC aerosol aging in northern PSEA can change the columnar aerosol optical properties and aerosol type, as well as aerosol chemical components. Therefore, when one wants to perform a radiative forcing calculation for this region, those factors should be carefully considered.

An improved aerosol composition model that includes BC, BrC, DU, AS, and aerosol water uptake (AW) could effectively describe the variability of the aerosol aging and transport processes in PSEA. However, both the aerosol type classification method and chemical component retrieval method are dependent on inversion products and the modeling assumptions. In this study, we selected the Maxwell–Garnett mixing assumption for the aerosol component retrieval, which could yield different results with other mixing assumptions (e.g., Bruggeman and volume average mixing assumption) (Dey et al. 2006; Xie et al. 2014, 2017). The aerosol refractive index was similar for the DU and AS aerosols (Table 1), which could cause confusion in the component retrieval results. Thus, further improvements of algorithms and observations for acquiring better information content and more reliable results are currently underway.

Supplementary Information The online version contains supplementary material available at https://doi.org/10.1007/s11869-021-01119-2.

Acknowledgements The authors thank the AERONET team for calibrating and maintaining instrumentation and processing these data. The authors also thank the AERONET site managers for their effort in establishing and maintaining Son La, Chiang Mai, Ubon Ratchathani, Silpakorn Univ, Bac Lieu, and Doi Ang Khang stations. We thank Dr. Stephen Griffith for editing the manuscript.

Funding This work was supported by the Ministry of Science and Technology of Taiwan under grant no. MOST 108–2111-M-008–025.

References

Bahadur R, Praveen PS, Xu Y, Ramanathan V (2012) Solar absorption by elemental and brown carbon determined from spectral observations. Proc Natl Acad Sci 109:17366–17371

Bohren CF, Huffman DR (1998) Absorption and scattering of light by small particles. John Wiley & Sons.https://doi.org/10.1002/9783527618156

Boucher O, Randall D, Artaxo P, Bretherton C, Feingold G, Forster P, Kerminen V, Kondo Y, Liao H, Lohmann U (2013) Clouds and aerosols. Climate change 2013: the physical science basis. Contribution of Working Group I to the Fifth Assessment Report of the Intergovernmental Panel on Climate Change. Cambridge University Press, Cambridge, United Kingdom and New York, NY, USA, pp 571–657

Charlson RJ, Schwartz S, Hales J, Cess RD, Coakley JJ, Hansen J, Hofmann D (1992) Climate forcing by anthropogenic aerosols. Science 255:423–430

Chen LWA, Moosmüller H, Arnott WP, Chow JC, Watson JG, Susott RA, Babbitt RE, Wold CE, Lincoln EN, Hao WM (2006) Particle emissions from laboratory combustion of wildland fuels: in situ optical and mass measurements. Geophys Res Lett 33

Chen L-WA, Moosmüller H, Arnott WP, Chow JC, Watson JG, Susott RA, Babbitt RE, Wold CE, Lincoln EN, Hao WM (2007) Emissions from laboratory combustion of wildland fuels: emission factors and source profiles. Environ Sci Technol 41:4317–4325

Chen S, Russell LM, Cappa CD, Zhang X, Kleeman MJ, Kumar A, Liu D, Ramanathan V (2019) Comparing black and brown carbon absorption from AERONET and surface measurements at Wintertime Fresno. Atmos Environ 199:164–176

Chu J-E, Ha K-J (2016) Quantifying organic aerosol single scattering albedo over the tropical biomass burning regions. Atmos Environ 147:67–78

Dey S, Tripathi S, Singh RP, Holben B (2006) Retrieval of black carbon and specific absorption over Kanpur city, northern India during 2001–2003 using AERONET data. Atmos Environ 40:445–456

Dubovik O, Smirnov A, Holben B, King M, Kaufman Y, Eck T, Slutsker I (2000) Accuracy assessments of aerosol optical properties retrieved from Aerosol Robotic Network (AERONET) sun and sky radiance measurements. J Geophys Res Atmos 105:9791–9806

Chylek P, Wong J (1995) Effect of absorbing aerosols on global radiation budget. Geophys Res Lett 22:929–931

Esteve A, Highwood E, Morgan W, Allen G, Coe H, Grainger R, Brown P, Szpek K (2014) A study on the sensitivities of simulated aerosol optical properties to composition and size distribution using airborne measurements. Atmos Environ 89:517–524

Esteve A, Ogren J, Sheridan P, Andrews E, Holben B, Utrillas M (2012) Sources of discrepancy between aerosol optical depth obtained from AERONET and in-situ aircraft profiles. Atmos Chem Phys 12:2987

Feng Y, Ramanathan V, Kotamarthi V (2013) Brown carbon: a significant atmospheric absorber of solar radiation? Atmos Chem Phys Discuss 13

Forster P, Ramaswamy V, Artaxo P, Berntsen T, Betts R, Fahey DW, Haywood J, Lean J, Lowe DC, Myhre G (2007) Changes in atmospheric constituents and in radiative forcing. Chapter 2, In Climate Change 2007. The Physical Science Basis

Giles DM, Holben BN, Eck TF, Sinyuk A, Smirnov A, Slutsker I, Dickerson R, Thompson A, Schafer J (2012) An analysis of AERONET aerosol absorption properties and classifications representative of aerosol source regions. J Geophys Res Atmos 117

Holben BN, Eck TF, Slutsker I, Tanré D, Buis JP, Setzer A, Vermote E, Reagan JA, Kaufman YJ, Nakajima T, Lavenu F, Jankowiak I, Smirnov A (1998) AERONET—a federated instrument network and data archive for aerosol characterization. Remote Sens Environ 66:1–16

Holben BN, Tanre D, Smirnov A, Eck T, Slutsker I, Abuhassan N, Newcomb W, Schafer J, Chatenet B, Lavenu F (2001) An emerging ground-based aerosol climatology: aerosol optical depth from AERONET. J Geophys Res Atmos 106:12067–12097

Hassan T, Moosmüller H, Chung CE (2015) Coefficients of an analytical aerosol forcing equation determined with a Monte-Carlo radiation model. J Quant Spectrosc Radiat Transfer 164:129–136

Hess M, Koepke P, Schult I (1998) Optical properties of aerosols and clouds: the software package OPAC. Bull Am Meteor Soc 79:831–844. https://doi.org/10.1175/1520-0477(1998)079%3c0831:opoaac%3e2.0.co;2

IPCC (2013) Working Group I Contribution to the IPCC Fifth Assessment Report: Climate Change 2013: The Physical Science Basis, Summary for Policymakers IPCC, UN

Lee J, Hsu NC, Bettenhausen C, Sayer AM, Seftor CJ, Jeong M-J, Tsay S-C, Welton EJ, Wang S-H, Chen W-N (2016) Evaluating the height of biomass burning smoke aerosols retrieved from synergistic use of multiple satellite sensors over Southeast Asia. Aerosol Air Qual Res 16:2831–2842

Li Z, Gu X, Wang L, Li D, Xie Y, Li K, Dubovik O, Schuster G, Goloub P, Zhang Y (2013) Aerosol physical and chemical properties retrieved from ground-based remote sensing measurements during heavy haze days in Beijing winter. Atmos Chem Phys 13:10171–10183

Lin N-H, Sayer AM, Wang S-H, Loftus AM, Hsiao T-C, Sheu G-R, Hsu NC, Tsay S-C, Chantara S (2014) Interactions between biomass-burning aerosols and clouds over Southeast Asia: current status, challenges, and perspectives. Environ Pollut 195:292–307

Lin N-H, Tsay S-C, Maring HB, Yen M-C, Sheu G-R, Wang S-H, Chi KH, Chuang M-T, Ou-Yang C-F, Fu JS, Reid JS, Lee C-T, Wang L-C, Wang J-L, Hsu CN, Sayer AM, Holben BN, Chu Y-C, Nguyen XA, Sopajaree K, Chen S-J, Cheng M-T, Tsuang B-J, Tsai C-J, Peng C-M, Schnell RC, Conway T, Chang C-T, Lin K-S, Tsai YI, Lee W-J, Chang S-C, Liu J-J, Chiang W-L, Huang S-J, Lin T-H, Liu G-R (2013) An overview of regional experiments on biomass burning aerosols and related pollutants in Southeast Asia:

from Base-Asia and the Dongsha experiment to 7-Seas. Atmos Environ 78:1–19

Moosmüller H, Chakrabarty R (2011) Simple analytical relationships between Ångström coefficients of aerosol extinction, scattering, absorption, and single scattering albedo. Atmos Chem Phys 11:10677–10680

Moosmüller H, Chakrabarty R, Arnott W (2009) Aerosol light absorption and its measurement: a review. J Quant Spectrosc Radiat Transfer 110:844–878

Pani SK, Lin N-H, Chantara S, Wang S-H, Khamkaew C, Prapamontol T, Janjai S (2018) Radiative response of biomass-burning aerosols over an urban atmosphere in northern Peninsular Southeast Asia. Sci Total Environ 633:892–911

Pani SK, Wang S-H, Lin N-H, Lee C-T, Tsay S-C, Holben BN, Janjai S, Hsiao T-C, Chuang M-T, Chantara S (2016) Radiative effect of springtime biomass-burning aerosols over Northern Indochina during 7-Seas/Baseline 2013 campaign. Aerosol Air Qual Res 16:2802–2817

Punsompong P, Pani SK, Wang S-H, Pham TTB (2021) Assessment of biomass-burning types and transport over Thailand and the associated health risks. Atmos Environ 247:118176

Russell P, Bergstrom R, Shinozuka Y, Clarke A, DeCarlo P, Jimenez J, Livingston J, Redemann J, Dubovik O, Strawa A (2010) Absorption Angstrom exponent in AERONET and related data as an indicator of aerosol composition. Atmos Chem Phys 10:1155–1169

Schuster GL, Dubovik O, Holben BN, Clothiaux EE (2005) Inferring black carbon content and specific absorption from Aerosol Robotic Network (AERONET) aerosol retrievals. J Geophys Res Atmos 110

Sinyuk A, Holben BN, Eck TF, Giles DM, Slutsker I, Korkin S, Schafer JS, Smirnov A, Sorokin M, Lyapustin A (2020) The AERONET Version 3 aerosol retrieval algorithm, associated uncertainties and comparisons to Version 2. Atmos Meas Tech 13:3375–3411

Tsay S-C, Maring HB, Lin N-H, Buntoung S, Chantara S, Chuang H-C, Gabriel PM, Goodloe CS, Holben BN, Hsiao T-C, Hsu NC, Janjai S, Lau WKM, Lee C-T, Lee J, Loftus AM, Nguyen AX, Nguyen CM, Pani SK, Pantina P, Sayer AM, Tao W-K, Wang S-H, Welton EJ, Wiriya W, Yen M-C (2016) Satellite-surface perspectives of air quality and aerosol-cloud effects on the environment: an overview of 7-Seas/Baseline. Aerosol Air Qual Res 16:2581–2602

Valenzuela A, Reid JP, Bzdek BR, Orr-Ewing AJ (2018) Accuracy required in measurements of refractive index and hygroscopic response to reduce uncertainties in estimates of aerosol radiative forcing efficiency. J Geophys Res Atmos 123:6469–6486

Van Beelen A, Roelofs G, Hasekamp O, Henzing J, Röckmann T (2014) Estimation of aerosol water and chemical composition from AERONET sun–sky radiometer measurements at Cabauw, the Netherlands. Atmos Chem Phys 14:5969–5987

Wang S-H, Lin N-H, Chou M-D, Woo J-H (2007) Estimate of radiative forcing of Asian biomass-burning aerosols during the period of trace-P. J Geophys Res 112:D10222

Wang S-H, Welton EJ, Holben BN, Tsay S-C, Lin N-H, Giles D, Stewart SA, Janjai S, Nguyen XA, Hsiao T-C (2015) Vertical distribution and columnar optical properties of springtime biomass-burning aerosols over Northern Indochina during 2014 7-Seas campaign. Aerosol Air Qual Res 15:2037–2050

Xie Y, Li Z, Li L, Wang L, Li D, Chen C, Li K, Xu H (2014) Study on influence of different mixing rules on the aerosol components retrieval from ground-based remote sensing measurements. Atmos Res 145:267–278

Xie Y, Li Z, Zhang Y, Zhang Y, Li D, Li K, Xu H, Wang Y, Chen X, Schauer J (2017) Estimation of atmospheric aerosol composition from ground-based remote sensing measurements of sun-sky radiometer. J Geophys Res Atmos 122:498–518

Yen M-C, Peng C-M, Chen T-C, Chen C-S, Lin N-H, Tzeng R-Y, Lee Y-A, Lin C-C (2013) Climate and weather characteristics in association with the active fires in Northern Southeast Asia and spring air pollution in Taiwan during 2010 7-Seas/Dongsha experiment. Atmos Environ 78:35–50